Optical Sensing of Fractional Quantum Hall Effect in Graphene

Alexander Popert, Yuya Shimazaki, Martin Kroner, Kenji Watanabe, Takashi Taniguchi, Ataç Imamoğlu, and Tomasz Smoleński*
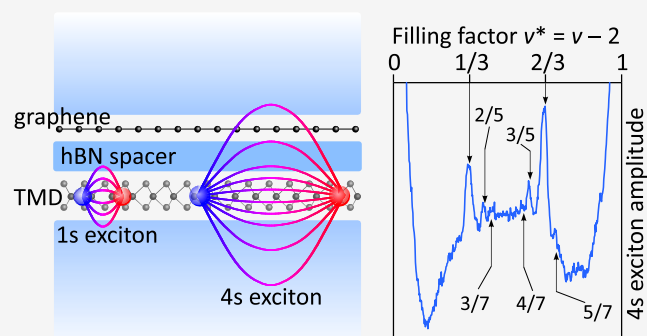
Read Online

ACCESS | Metrics & More | Article Recommendations | Supporting Information

ABSTRACT: Graphene and its heterostructures provide a unique and versatile playground for explorations of strongly correlated electronic phases, ranging from unconventional fractional quantum Hall (FQH) states in a monolayer system to a plethora of superconducting and insulating states in twisted bilayers. However, the access to those fascinating phases has been thus far entirely restricted to transport techniques, due to the lack of a robust energy bandgap that makes graphene hard to access optically. Here we demonstrate an all-optical, noninvasive spectroscopic tool for probing electronic correlations in graphene using excited Rydberg excitons in an adjacent transition metal dichalcogenide monolayer. These excitons are highly susceptible to the compressibility of graphene electrons, allowing us to detect the formation of odd-denominator FQH states at high magnetic fields. Owing to its submicron spatial resolution, the technique we demonstrate circumvents spatial inhomogeneities and paves the way for optical studies of correlated states in optically inactive atomically thin materials.

KEYWORDS: *graphene, quantum Hall effect, optical sensing, correlated electrons, Rydberg excitons, van der Waals heterostructures*

S ince their first mechanical exfoliation from a bulk graphite crystal,[1−3] graphene monolayers have emerged as a fascinating and promising experimental platform for explorations of two-dimensional electron systems (2DES). Owing to linear band dispersion, graphene subjected to an external magnetic field B features an unusual sequence of anharmonically spaced Landau levels (LLs).[4] Strong quenching of kinetic energy together with reduced dielectric screening compared to conventional GaAs-based 2DES markedly enhances the stability of fractional quantum Hall (FQH) states—correlated electronic states arising in partially filled LLs due to electron–electron interactions.[5−7] FQH states typically emerge at odd-denominator fractional filling factors $\nu = n/(2pn \pm 1)$ for integers n and p.[8−10] Advances in the fabrication of graphene-based devices have further enabled the observation of even more exotic correlated phases, including even-denominator FQH states,[11,12] fractal FQH states originating from a superlattice moiré potential in angle-aligned graphene-hexagonal boron-nitride (hBN) heterostructures,[13−15] as well as superconducting and correlated Chern insulator phases in magic-angle twisted bilayer graphene (MATBG).[16−20]

Most of the prior investigations of strong electronic correlations in graphene have been limited to transport experiments. This is due to the lack of a robust bandgap, which hinders usage of interband optical transitions to probe the formation of incompressible or correlated states in a similar way as has been done for GaAs-based quantum wells.[21−26]

This motivates the following question: Can such states in graphene be investigated by purely optical means? Optical spectroscopy with its high spatial resolution allows for circumventing both the influence of device edges and disorder-related effects arising from inevitable spatial inhomogeneities introduced during assembly of van der Waals heterostructures. Furthermore, optical probes offer ultrafast access to correlated electronic states. They may therefore enable explorations of elusive correlated phases being thus far inaccessible in transport techniques.

Here, we demonstrate all-optical detection of the FQH effect in graphene with the use of a proximal transition metal dichalcogenide (TMD) monolayer. The utilized technique exploits the fact that Coulomb interactions between charge carriers in a TMD monolayer are highly susceptible to the dielectric environment.[27,28] This allows us to use excited Rydberg states of a TMD exciton as quantum proximity sensors for the compressibility of a 2DES in an adjacent layer, as first shown in refs 28−30. Owing to graphene's almost
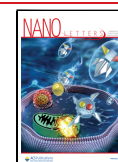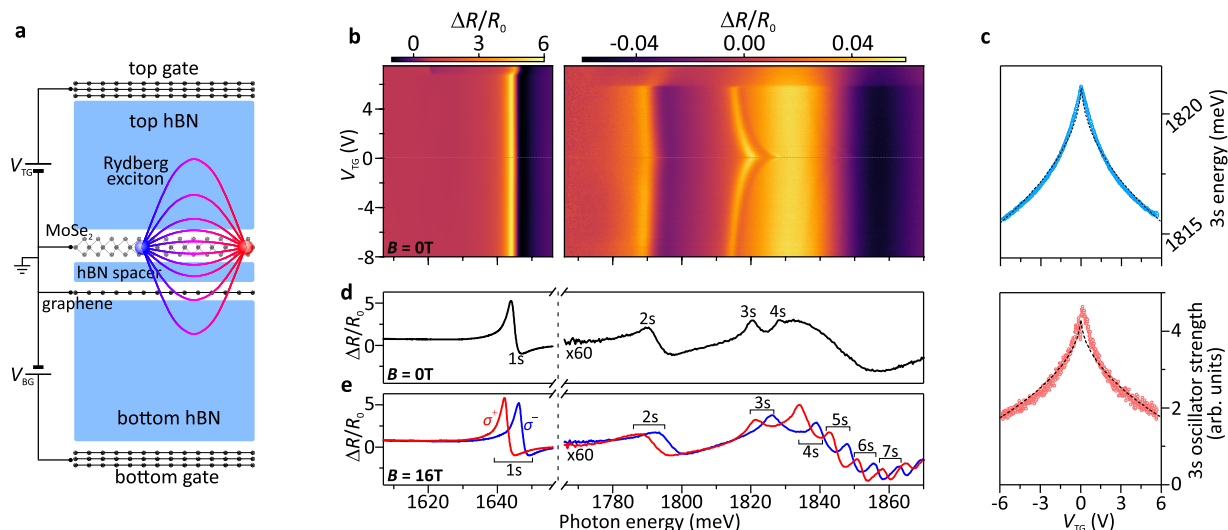
Figure 1. Sensing the compressibility of graphene electrons with Rydberg excitons. (a) Cartoon illustrating the layer structure of the sample region investigated in the main text. (b) V_{TG}-evolution of the zero-field $\Delta R/R_0$ spectra acquired at $V_{BG} \approx 0$ V and at $T \approx 4$ K in the spectral range of the ground exciton (left) and the excited Rydberg states (right). The graphene charge-neutrality point at $V_{TG} \approx 0$ V is marked by a horizontal dashed line. The onset of MoSe$_2$ monolayer doping occurs at $V_{TG} \approx 6$ V. (c) Voltage-dependent energy (top) and oscillator strength (bottom) of the 3s exciton obtained by fitting its line shape with a dispersive Lorentzian spectral profile. The dashed lines mark the fitted dependencies of the form $\propto 1 - a\sqrt{|n_e|}$ (where a is a fitting parameter) that correspond to the reduction of both quantities being proportional to the quantum capacitance $C_Q \propto \sqrt{|n_e|}$ that in turn determines graphene compressibility $\kappa \propto C_Q/n_e^2$. (d) Line cut through the maps in panel b at $V_{TG} \approx 0$ V. (e) Reflectance contrast spectra measured on the same spot at $B = 16$ T in two circular polarizations. Note that the Rydberg excitons are overlaid on a broad spectral feature stemming from the B-exciton of the MoSe$_2$ monolyer (see SI for details).

perfect electron−hole symmetry[4] and low light absorption coefficient,[31] this method does not affect the LL filling factor of the 2DES and hence constitutes a nondestructive probe for the correlations between the graphene electrons. The Rydberg exciton spectroscopy we implement is similarly sensitive to state-of-the-art transport techniques but is more versatile as it permits studying the FQH effect in simple device geometries with high spatial resolution and without requiring electrical currents.

The device we investigate consists of a graphene flake separated from a MoSe$_2$ monolayer by a thin hBN spacer (see Figure 1a). The spacer exhibits a spatially dependent thickness, in particular featuring hBN terraces of 1 or 5 monolayers (MLs). Unless otherwise stated, we exclusively explore the region with a 5 ML thick spacer in the main text [see Supporting Information (SI) for additional data obtained in other sample regions]. All investigated spots are located away from physical edges between various sample regions, ensuring that our findings are not affected by edge-related effects. The graphene-hBN-MoSe$_2$ structure is encapsulated between 40−50 nm thick hBN slabs and then embedded in top and bottom graphite layers, which enable us to control the carrier density by applying gate voltages (V_{TG} and V_{BG}). The sample is loaded into a dilution refrigerator equipped with fiber-based optical access and a heater allowing for reaching base temperatures ranging from 80 mK to 20 K (see SI). The optical response of the TMD monolayer is analyzed by means of reflectance contrast $\Delta R/R_0 = (R - R_0)/R_0$ spectroscopy, where R denotes the white-light reflectance spectrum of the device, while R_0 corresponds to the background spectrum (see SI).

Figure 1b shows the V_{TG}-evolution of the reflectance contrast spectrum of our device acquired at $T = 4$ K and $B = 0$. Due to the sizable energy offset between the graphene Dirac point and the MoSe$_2$ conduction band edge,[32] electron

doping of the TMD only occurs at $V_{TG} \gtrsim 5$ V. This is where we observe attractive and repulsive Fermi-polarons for the 1s exciton.[33,34] In this work, we focus on the opposite regime $V_{TG} \lesssim 5$ V, where the TMD remains charge neutral as carriers are introduced exclusively to the graphene layer.

Under these conditions, the energy of the MoSe$_2$ 1s exciton is almost completely independent of the changes in graphene doping density n_e. This is due to extremely tight binding of this exciton state[35] that renders its optical transition insensitive to screening by graphene electrons. More specifically, the screening-induced decrease of the 1s binding energy (ΔE_{1s}) is perfectly compensated by a corresponding reduction of the quasiparticle bandgap (ΔE_g) of the TMD monolayer.[30,36−38] Such a compensation does not hold for the excited Rydberg exciton states ns (with $n = 2, 3,...$), which feature larger Bohr radii and smaller binding energies.[39,40] As a consequence, we observe a prominent red-shift of the Rydberg exciton energies $\Delta E_g - \Delta E_{ns} < 0$ which is particularly well-resolved for the 3s exciton. This energy shift is directly proportional to the quantum capacitance $C_Q = e^2 \partial n_e/\partial E_F$ of graphene electrons which increases nonlinearly with the doping density, scaling as $\sqrt{|n_e|}$ due to the linear dispersion of graphene.[2−4] This behavior is qualitatively consistent with a long-wavelength approximation[4,41] for the screening of Rydberg excitons that holds[30] as long as their Bohr radii remain much larger than the inverse Fermi wavevector in graphene. In parallel to the reduction of ΔE_{ns}, the oscillator strength of the Rydberg state also decreases $\propto \sqrt{|n_e|}$, as can be seen in Figure 1c. These findings demonstrate that both the energy and the oscillator strength of the Rydberg excitons can be used as quantitative probes of the electronic compressibility $\kappa \propto C_Q/n_e^2$ of proximal graphene.
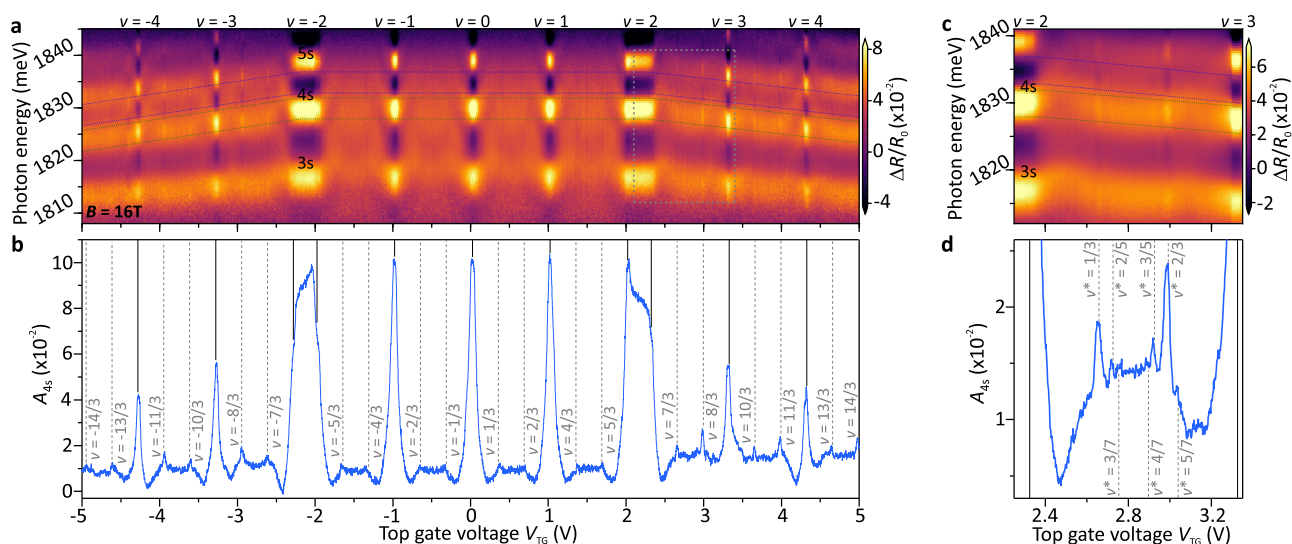
Figure 2. Optical probing of FQH states in graphene. (a) V_{TG}-evolution of the reflectance contrast spectra measured in Rydberg-exciton spectral range at $B = 16$ T, $T = 80$ mK, and for $V_{BG} = 0$ V. (b) V_{TG}-dependent amplitude of the 4s exciton determined as a difference between $\Delta R/R_0$ averaged over two 4-meV-wide spectral windows around the 4s resonance (marked by blue and green dashed lines in panel a). The vertical solid (dashed) lines mark the subsequent integer (fractional) filling factors of graphene LLs. (c) $\Delta R/R_0$ spectra acquired in a narrower voltage range corresponding to $2 \lesssim \nu \lesssim 3$ (indicated by the dotted rectangle in panel a) with improved signal-to-noise ratio. (d) The V_{TG}-dependent amplitude of the 4s exciton determined in a similar way as in panel b based on the spectra in panel c. The amplitude exhibits several prominent maxima revealing a multitude of FQH states with denominators of 3, 5, and 7 (as indicated by the vertical dashed lines).

In order to exploit Rydberg exciton spectroscopy to study electronic correlations, we apply a strong magnetic field $B = 16$ T that leads to LL formation and thereby quenches the kinetic energy of graphene electrons. Concurrent quantization of motion of the TMD electrons and holes provides additional confinement to the Rydberg excitons. As a consequence, Rydberg excitons at $B = 16$ T are considerably stronger compared to their zero-field counterparts (see Figure 1d,e), which in turn improves the overall sensitivity of our sensing scheme. These excitons also remain bound for markedly higher principle quantum numbers exceeding $n \approx 5$, for which the energy splitting between consecutive Rydberg states approaches the sum of electron and hole cyclotron energies in the TMD monolayer.[39,40]

Under the influence of a high B-field, the Rydberg states exhibit a qualitatively different response to changes in graphene doping density. We show this in Figure 2a which displays V_{TG}-dependent reflectance contrast spectra in the 3s–6s energy range. The spectra were acquired at $T = 80$ mK using low white-light power ∼9 nW as well as almost cross-linearly polarized excitation and collection beams (see SI). This allows us to further increase the amplitude of optical Rydberg transitions.

Strikingly, the reflectance contrast amplitude A_{ns} of the Rydberg excitons undergoes periodic oscillations with V_{TG}, which arise due to the Landau-quantization of the graphene density of states. In general, at noninteger fillings the electrons are compressible and thereby efficiently screen the Rydberg excitons, which in turn quenches their optical response. Conversely, when the Fermi level lies in the gap between the LLs, the electronic state becomes incompressible, which results in a prominent enhancement of the amplitude of Rydberg transitions at subsequent integer filling factors. The A_{ns} maxima at $\nu = \pm 2$ extend over a considerably broader V_{TG} range than those at other fillings. This is a consequence of nonuniform energy spacing of graphene LLs that are grouped into

manifolds consisting of four LLs.[4−6] The spin and valley degeneracy of LLs belonging to each manifold is lifted predominantly by many-body exchange interactions between the electrons,[42] but the resulting splitting still remains more than an order of magnitude smaller than the cyclotron gaps between subsequent manifolds. For $\nu = \pm 2$, the LL spacing is

$$\Delta E_{\pm 2} = \sqrt{2e\hbar v_F^2 B} \approx 0.16 \text{ eV}$$ at $B = 16$ T, where $\hbar$ denotes the reduced Planck constant, and v_F is the Fermi velocity. To cross such a sizable energy gap, we need to increase the gate voltage by $\Delta V_{TG} \approx 0.4$ V, which leads to the excessive width of $\nu = \pm 2$ peaks. The analysis of the resulting displacement of other IQH features (see SI) allows us to extract $v_F = (1.1 \pm 0.1) \times 10^6$ m/s, which is consistent with previous reports for hBN-encapsulated graphene.[43]

Remarkably, the data in Figure 2a also feature another sequence of weaker enhancements of Rydberg exciton amplitude, hinting at the presence of additional incompressible states at fractional fillings. To get better insight into the nature of those states, we extract an effective measure for the 4s exciton amplitude defined as $A_{4s} = \langle \Delta R/R_0 \rangle_{4s}^{peak} - \langle \Delta R/R_0 \rangle_{4s}^{dip}$, where the two terms represent the reflection contrast spectrally averaged over the peak and the dip around the 4s resonance (see SI). This procedure allows us to reduce the common mode noise, originating, e.g., from the long-term fluctuations in our setup. The resulting V_{TG}-dependence of A_{4s} (Figure 2b) indeed exhibits pronounced peaks at voltages precisely corresponding to either 1/3 or 2/3 fillings of all subsequent LLs, which in turn correspond to the most robust odd-denominator FQH states with the largest quasiparticle energy gaps.[10,44] This observation provides unequivocal evidence for the formation of FQH states in graphene. Interestingly, the FQH states at the first excited LL1 manifold ($2 < |\nu| < 6$) give rise to significantly stronger Rydberg exciton amplitude maxima as compared to those at LL0 ($|\nu| < 2$); this is unexpected as prior transport experiments have demonstrated that FQH states at LL0 are slightly more robust.[44] Temper-
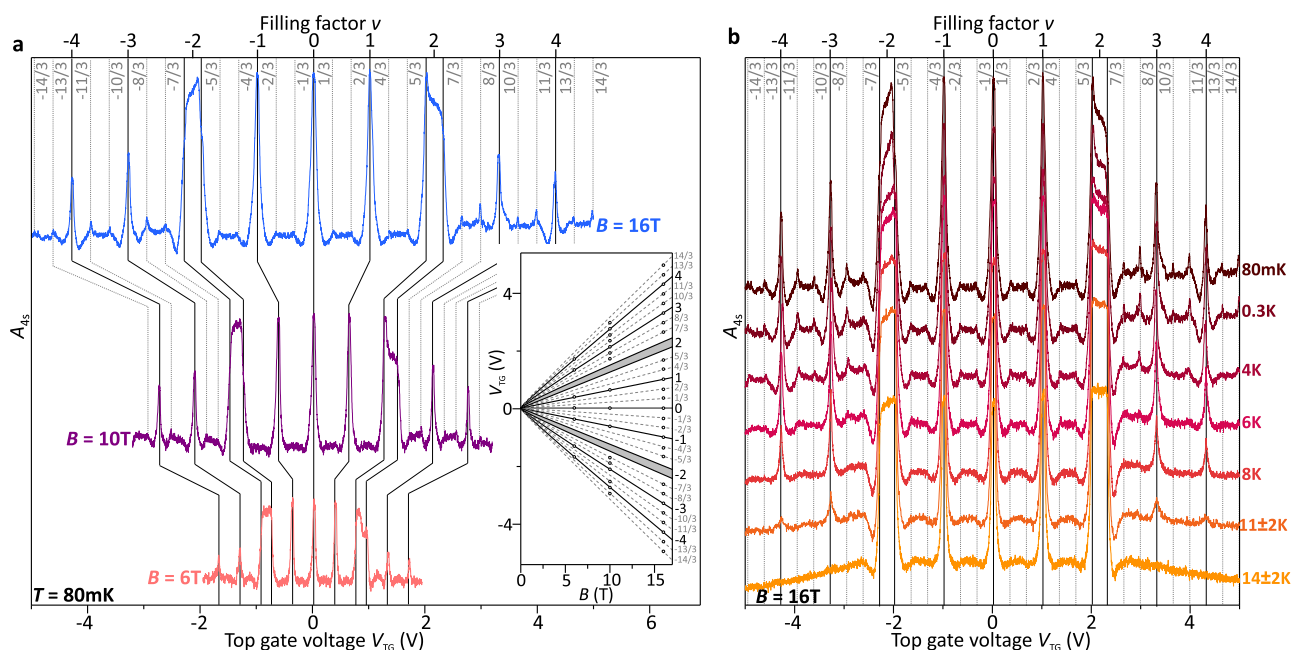
Figure 3. Magnetic field and temperature dependence of FQH states in graphene. (a) V_{TG}-dependent amplitude of the 4s exciton acquired at $T = 80$ mK, $V_{BG} = 0$ V, but at different $B = 16$, 10, and 6 T. The vertical solid (dashed) lines indicate integer (fractional) filling factors. Inset: V_{TG} corresponding to subsequent integer and fractional filling factors determined as a function of B by fitting the positions of the 4s exciton amplitude maxima with phenomenological, Gaussian profiles (see SI). Solid and dashed lines represent the fit of the data with dependencies described in the text that form a LL fan chart. (b) V_{TG}-dependent amplitude of the 4s exciton acquired at $B = 16$ T, $V_{BG} = 0$ V, but for different temperatures. In both panels the curves are vertically offset for clarity.

ature-dependent measurements which we discuss below indicate that the activation gaps of FQH states at LL0 and LL1 are also comparable in our sample. This suggests that the striking difference in FQH visibility at $|\nu| < 2$ and $|\nu| > 2$ is an inherent property of the Rydberg exciton sensing scheme we employ. A detailed description of the underlying physical mechanism remains, however, beyond the scope of this work.

Taking advantage of the fact that FQH signatures are particularly well-resolved at $2 < \nu < 3$, we examine this filling-factor range more closely by averaging reflectance spectra acquired with longer integration time, which allows us to further improve the signal-to-noise ratio. As shown in Figure 2c,d, this reveals the presence of even fainter A_{4s} maxima corresponding to FQH states with larger denominators of 5 and 7. We emphasize that the number of fractional fillings we observe is comparable to the highest odd denominators that have been previously reported for FQH states in graphene using transport studies at similar B-fields.[7,44] This suggests that Rydberg exciton spectroscopy yields a sensitivity that is similar to state-of-the-art transport techniques.

Having established optical access to FQH states in graphene, we investigate their robustness to changes in system parameters. Figure 3a presents the voltage-dependent amplitude of 4s resonance measured at the same $T = 80$ mK, but at different B values. As expected, when lowering the B-field, signatures of FQH states become less prominent and are no longer discernible at $B = 6$ T. In parallel, owing to reduced LL degeneracy (being proportional to B), the voltage gaps between subsequent Rydberg amplitude maxima become narrower. To analyze this effect quantitatively, we fit the positions of the maxima with a set of dependencies obtained within the parallel-plate capacitor model (see SI), which forms a graphene LL fan diagram. This allows us to extract the basic parameters of the graphene monolayer: in addition to ν_F

introduced earlier, we find the $V_{TG} \approx 22$ mV corresponding to graphene charge-neutrality as well as the voltage change $\Delta V_{TG} \approx 62.5$ mV/T required to fill a LL at $B = 1$ T. The latter value can be used to determine the out-of-plane hBN dielectric constant to be $\varepsilon_{hBN}^{\perp} = 3.1 \pm 0.2$, which is consistent with previous reports.[30,45] We emphasize that this model is used for assignment of all IQH and FQH states in our work. Its perfect agreement with the data further corroborates our identification of the amplitude maxima as FQH states and demonstrates in particular that fractal Hofstadter states, which could arise from a moiré superlattice between hBN and graphene, play no role in our device.[13−15] We further exclude any influence from Landau-quantization of the top and bottom graphite gates[46] on the investigated effects by performing analogous V_{TG}-dependent reflectance measurements at various back gate voltages (see SI).

The visibility of FQH states is also reduced at elevated temperatures. Figure 3b shows a set of Rydberg optical responses acquired at fixed $B = 16$ T, but for various device temperatures. The peaks associated with $n/3$ FQH states disappear around $T \approx 4−6$ K for all investigated LLs at $|\nu| < 5$, which corresponds to activation energy gaps a few times smaller than the highest gaps reported for the same FQH states in previous transport studies of graphene at comparable B-fields.[44] We also note that the signatures of FQH states are sensitive to the optical excitation power, becoming sizeably suppressed upon increasing the power to a few tens of nW. This stems both from small but finite graphene light absorption and from power-induced quenching of Rydberg exciton transitions in a TMD monolayer (see SI for details).

Although spatial mapping of the FQH effect across the sample remains beyond the scope of this work, we underline that our findings have been reproduced on a few different spots in the investigated sample region featuring a 5 ML thick hBN

spacer between the graphene and the TMD monolayer. Interestingly, we have not been able to detect FQH states in the 1 ML thick spacer region with similar acquisition time. This is most likely a consequence of the strongly suppressed amplitude of Rydberg transitions in this region even for integer fillings, which in turn reduces the sensitivity of our optical probing technique. Given that Rydberg resonances also become insensitive to the graphene compressibility for spacer thicknesses approaching their Bohr radii limited by the magnetic length, these findings illustrate that there is an optimal spacer thickness which maximizes the visibility of FQH states for any given B (see SI). Finally, we emphasize that we have also observed analogous signatures of the formation of FQH states in Bernal-stacked bilayer graphene with a 5 ML thick spacer, which further confirms the applicability of our detection scheme for various two-dimensional materials.

The experiments we report in this work establish the TMD monolayer as a nondestructive optical sensor for the FQH states in an adjacent graphene layer. This remote sensing scheme based on Rydberg excitons demonstrates the feasibility of optical investigations of strong electronic correlations in atomically thin materials that are otherwise optically inaccessible, e.g., indirect bandgap semiconductors or MATBG. In parallel, Rydberg exciton spectroscopy offers excellent spatial resolution determined by the submicron diffraction limit for the optical spot size. Compared to conventional transport techniques, this allows us to greatly reduce the influence of spatial inhomogeneities that are inherent to most van der Waals heterostructures. This may in turn pave the way for the observation of novel exotic correlated phases, such as fractional Chern insulators[47,48] in MATBG which have been demonstrated to be very sensitive to twist-angle variations occurring at ∼μm length scales.[18]

Remarkably, our approach also provides ultrafast temporal resolution determined by the picosecond-long exciton lifetime. This brings up a unique opportunity to explore nonequilibrium dynamics of strongly correlated electronic phases that is beyond the reach of any transport experiments. Another promising extension of our optical detection scheme would be to replace the sensing layer with a TMD bilayer structure hosting optical excitations that are coherent superpositions of intra- and interlayer excitons.[49,50] Due to the finite dipole moment of these hybrid excitons, we expect this scheme to allow for optical explorations of electronic correlations with drastically enhanced sensitivity.

■ ASSOCIATED CONTENT

Data Availability Statement
The data that support the findings of this paper are available at the ETH Research Collection (http://hdl.handle.net/20.500.11850/569263).

SI Supporting Information
The Supporting Information is available free of charge at https://pubs.acs.org/doi/10.1021/acs.nanolett.2c02000.

> Further details of the device fabrication and experimental setup, characterization of gate-voltage response of the device and calibration of electron doping density, description of data analysis procedures used for normalization and processing of the reflectance spectra, discussion of the sensitivity of the Rydberg exciton sensing scheme, and further experimental data obtained

in different regions of the device as well as for various out-of-plane electric fields (PDF)

■ AUTHOR INFORMATION

Corresponding Author
Tomasz Smoleński − *Institute for Quantum Electronics, ETH Zürich, CH-8093 Zürich, Switzerland;* ◉ orcid.org/0000-0002-4706-7777; Email: tomaszs@phys.ethz.ch

Authors
Alexander Popert − *Institute for Quantum Electronics, ETH Zürich, CH-8093 Zürich, Switzerland*

Yuya Shimazaki − *Institute for Quantum Electronics, ETH Zürich, CH-8093 Zürich, Switzerland; Center for Emergent Matter Science, RIKEN, Wako, Saitama 351-0198, Japan*

Martin Kroner − *Institute for Quantum Electronics, ETH Zürich, CH-8093 Zürich, Switzerland*

Kenji Watanabe − *Research Center for Functional Materials, National Institute for Materials Science, Tsukuba, Ibaraki 305-0044, Japan;* ◉ orcid.org/0000-0003-3701-8119

Takashi Taniguchi − *International Center for Materials Nanoarchitectonics, National Institute for Materials Science, Tsukuba, Ibaraki 305-0044, Japan;* ◉ orcid.org/0000-0002-1467-3105

Ataç Imamoğlu − *Institute for Quantum Electronics, ETH Zürich, CH-8093 Zürich, Switzerland*

Complete contact information is available at:
https://pubs.acs.org/10.1021/acs.nanolett.2c02000

Notes
The authors declare no competing financial interest.

■ REFERENCES

(1) Novoselov, K. S.; Geim, A. K.; Morozov, S. V.; Jiang, D.; Zhang, Y.; Dubonos, S. V.; Grigorieva, I. V.; Firsov, A. A. Electric Field Effect in Atomically Thin Carbon Films. *Science* **2004**, *306*, 666−669.

(2) Novoselov, K. S.; Geim, A. K.; Morozov, S. V.; Jiang, D.; Katsnelson, M. I.; Grigorieva, I. V.; Dubonos, S. V.; Firsov, A. A. Two-dimensional gas of massless Dirac fermions in graphene. *Nature* **2005**, *438*, 197−200.

(3) Geim, A. K.; Novoselov, K. S. The rise of graphene. *Nat. Mater.* **2007**, *6*, 183−191.

(4) Das Sarma, S.; Adam, S.; Hwang, E. H.; Rossi, E. Electronic transport in two-dimensional graphene. *Rev. Mod. Phys.* **2011**, *83*, 407−470.

(5) Du, X.; Skachko, I.; Duerr, F.; Luican, A.; Andrei, E. Y. Fractional quantum Hall effect and insulating phase of Dirac electrons in graphene. *Nature* **2009**, *462*, 192−195.

(6) Bolotin, K. I.; Ghahari, F.; Shulman, M. D.; Stormer, H. L.; Kim, P. Observation of the fractional quantum Hall effect in graphene. *Nature* **2009**, *462*, 196−199.

(7) Zeng, Y.; Li, J. I. A.; Dietrich, S. A.; Ghosh, O. M.; Watanabe, K.; Taniguchi, T.; Hone, J.; Dean, C. R. High-Quality Magnetotransport

in Graphene Using the Edge-Free Corbino Geometry. *Phys. Rev. Lett.* **2019**, *122*, 137701.

(8) Tsui, D. C.; Stormer, H. L.; Gossard, A. C. Two-Dimensional Magnetotransport in the Extreme Quantum Limit. *Phys. Rev. Lett.* **1982**, *48*, 1559−1562.

(9) Laughlin, R. B. Anomalous Quantum Hall Effect: An Incompressible Quantum Fluid with Fractionally Charged Excitations. *Phys. Rev. Lett.* **1983**, *50*, 1395−1398.

(10) Stormer, H. L.; Tsui, D. C.; Gossard, A. C. The fractional quantum Hall effect. *Rev. Mod. Phys.* **1999**, *71*, S298−S305.

(11) Li, J. I. A.; Tan, C.; Chen, S.; Zeng, Y.; Taniguchi, T.; Watanabe, K.; Hone, J.; Dean, C. R. Even-denominator fractional quantum Hall states in bilayer graphene. *Science* **2017**, *358*, 648−652.

(12) Zibrov, A. A.; Spanton, E. M.; Zhou, H.; Kometter, C.; Taniguchi, T.; Watanabe, K.; Young, A. F. Even-denominator fractional quantum Hall states at an isospin transition in monolayer graphene. *Nat. Phys.* **2018**, *14*, 930−935.

(13) Ponomarenko, L. A.; et al. Cloning of Dirac fermions in graphene superlattices. *Nature* **2013**, *497*, 594−597.

(14) Dean, C. R.; Wang, L.; Maher, P.; Forsythe, C.; Ghahari, F.; Gao, Y.; Katoch, J.; Ishigami, M.; Moon, P.; Koshino, M.; Taniguchi, T.; Watanabe, K.; Shepard, K. L.; Hone, J.; Kim, P. Hofstadter's butterfly and the fractal quantum Hall effect in moiré superlattices. *Nature* **2013**, *497*, 598−602.

(15) Yu, G. L.; et al. Hierarchy of Hofstadter states and replica quantum Hall ferromagnetism in graphene superlattices. *Nat. Phys.* **2014**, *10*, 525−529.

(16) Cao, Y.; Fatemi, V.; Demir, A.; Fang, S.; Tomarken, S. L.; Luo, J. Y.; Sanchez-Yamagishi, J. D.; Watanabe, K.; Taniguchi, T.; Kaxiras, E.; Ashoori, R. C.; Jarillo-Herrero, P. Correlated insulator behaviour at half-filling in magic-angle graphene superlattices. *Nature* **2018**, *556*, 80−84.

(17) Cao, Y.; Fatemi, V.; Fang, S.; Watanabe, K.; Taniguchi, T.; Kaxiras, E.; Jarillo-Herrero, P. Unconventional superconductivity in magic-angle graphene superlattices. *Nature* **2018**, *556*, 43−50.

(18) Uri, A.; Grover, S.; Cao, Y.; Crosse, J. A.; Bagani, K.; Rodan-Legrain, D.; Myasoedov, Y.; Watanabe, K.; Taniguchi, T.; Moon, P.; Koshino, M.; Jarillo-Herrero, P.; Zeldov, E. Mapping the twist-angle disorder and Landau levels in magic-angle graphene. *Nature* **2020**, *581*, 47−52.

(19) Stepanov, P.; Das, I.; Lu, X.; Fahimniya, A.; Watanabe, K.; Taniguchi, T.; Koppens, F. H.; Lischner, J.; Levitov, L.; Efetov, D. K. Untying the insulating and superconducting orders in magic-angle graphene. *Nature* **2020**, *583*, 375−378.

(20) Liu, X.; Wang, Z.; Watanabe, K.; Taniguchi, T.; Vafek, O.; Li, J. I. A. Tuning electron correlation in magic-angle twisted bilayer graphene using Coulomb screening. *Science* **2021**, *371*, 1261−1265.

(21) Heiman, D.; Goldberg, B. B.; Pinczuk, A.; Tu, C. W.; Gossard, A. C.; English, J. H. Optical Anomalies of the Two-Dimensional Electron Gas in the Extreme Magnetic Quantum Limit. *Phys. Rev. Lett.* **1988**, *61*, 605−608.

(22) Turberfield, A. J.; Haynes, S. R.; Wright, P. A.; Ford, R. A.; Clark, R. G.; Ryan, J. F.; Harris, J. J.; Foxon, C. T. Optical detection of the integer and fractional quantum Hall effects in GaAs. *Phys. Rev. Lett.* **1990**, *65*, 637−640.

(23) Meimberg, K.; Potemski, M.; Hawrylak, P.; Zhang, Y. H.; Ploog, K. Optically detected oscillations of screening by a two-dimensional electron gas in a magnetic field. *Phys. Rev. B* **1997**, *55*, 7685−7689.

(24) Potemski, M. Magneto-optics of a two-dimensional electron gas. *Phys. B: Condens. Matter* **1998**, *256−258*, 283−291.

(25) Yusa, G.; Shtrikman, H.; Bar-Joseph, I. Charged Excitons in the Fractional Quantum Hall Regime. *Phys. Rev. Lett.* **2001**, *87*, 216402.

(26) Byszewski, M.; Chwalisz, B.; Maude, D. K.; Sadowski, M. L.; Potemski, M.; Saku, T.; Hirayama, Y.; Studenikin, S.; Austing, D. G.; Sachrajda, A. S.; Hawrylak, P. Optical probing of composite fermions in a two-dimensional electron gas. *Nat. Phys.* **2006**, *2*, 239−243.

(27) Raja, A.; Waldecker, L.; Zipfel, J.; Cho, Y.; Brem, S.; Ziegler, J. D.; Kulig, M.; Taniguchi, T.; Watanabe, K.; Malic, E.; Heinz, T. F.;

Berkelbach, T. C.; Chernikov, A. Dielectric disorder in two-dimensional materials. *Nat. Nanotechnol.* **2019**, *14*, 832−837.

(28) Raja, A.; et al. Coulomb engineering of the bandgap and excitons in two-dimensional materials. *Nat. Commun.* **2017**, *8*, 15251.

(29) Xu, Y.; Liu, S.; Rhodes, D. A.; Watanabe, K.; Taniguchi, T.; Hone, J.; Elser, V.; Mak, K. F.; Shan, J. Correlated insulating states at fractional fillings of moiré superlattices. *Nature* **2020**, *587*, 214−218.

(30) Xu, Y.; Horn, C.; Zhu, J.; Tang, Y.; Ma, L.; Li, L.; Liu, S.; Watanabe, K.; Taniguchi, T.; Hone, J. C.; Shan, J.; Mak, K. F. Creation of moiré bands in a monolayer semiconductor by spatially periodic dielectric screening. *Nat. Mater.* **2021**, *20*, 645−649.

(31) Mak, K. F.; Sfeir, M. Y.; Wu, Y.; Lui, C. H.; Misewich, J. A.; Heinz, T. F. Measurement of the Optical Conductivity of Graphene. *Phys. Rev. Lett.* **2008**, *101*, 196405.

(32) Wilson, N. R.; Nguyen, P. V.; Seyler, K.; Rivera, P.; Marsden, A. J.; Laker, Z. P. L.; Constantinescu, G. C.; Kandyba, V.; Barinov, A.; Hine, N. D. M.; Xu, X.; Cobden, D. H. Determination of band offsets, hybridization, and exciton binding in 2D semiconductor hetero-structures. *Science Advances* **2017**, *3*, No. e1601832.

(33) Sidler, M.; Back, P.; Cotlet, O.; Srivastava, A.; Fink, T.; Kroner, M.; Demler, E.; Imamoglu, A. Fermi polaron-polaritons in charge-tunable atomically thin semiconductors. *Nat. Phys.* **2017**, *13*, 255−261.

(34) Efimkin, D. K.; MacDonald, A. H. Many-body theory of trion absorption features in two-dimensional semiconductors. *Phys. Rev. B* **2017**, *95*, 035417.

(35) Chernikov, A.; Berkelbach, T. C.; Hill, H. M.; Rigosi, A.; Li, Y.; Aslan, B.; Reichman, D. R.; Hybertsen, M. S.; Heinz, T. F. Exciton Binding Energy and Nonhydrogenic Rydberg Series in Monolayer WS$_2$. *Phys. Rev. Lett.* **2014**, *113*, 076802.

(36) Semkat, D.; Richter, F.; Kremp, D.; Manzke, G.; Kraeft, W. D.; Henneberger, K. Ionization equilibrium in an excited semiconductor: Mott transition versus Bose−Einstein condensation. *Phys. Rev. B* **2009**, *80*, 155201.

(37) Riis-Jensen, A. C.; Lu, J.; Thygesen, K. S. Electrically controlled dielectric band gap engineering in a two-dimensional semiconductor. *Phys. Rev. B* **2020**, *101*, No. 121110(R).

(38) Gjerding, M. N.; Cavalcante, L. S. R.; Chaves, A.; Thygesen, K. S. Efficient Ab Initio Modeling of Dielectric Screening in 2D van der Waals Materials: Including Phonons, Substrates, and Doping. *J. Phys. Chem. C* **2020**, *124*, 11609−11616.

(39) Goryca, M.; Li, J.; Stier, A. V.; Taniguchi, T.; Watanabe, K.; Courtade, E.; Shree, S.; Robert, C.; Urbaszek, B.; Marie, X.; Crooker, S. A. Revealing exciton masses and dielectric properties of monolayer semiconductors with high magnetic fields. *Nat. Commun.* **2019**, *10*, 4172.

(40) Molas, M. R.; Slobodeniuk, A. O.; Nogajewski, K.; Bartos, M.; Bala, Ł.; Babiński, A.; Watanabe, K.; Taniguchi, T.; Faugeras, C.; Potemski, M. Energy Spectrum of Two-Dimensional Excitons in a Nonuniform Dielectric Medium. *Phys. Rev. Lett.* **2019**, *123*, 136801.

(41) Hwang, E. H.; Das Sarma, S. Dielectric function, screening, and plasmons in two-dimensional graphene. *Phys. Rev. B* **2007**, *75*, 205418.

(42) Young, A. F.; Dean, C. R.; Wang, L.; Ren, H.; Cadden-Zimansky, P.; Watanabe, K.; Taniguchi, T.; Hone, J.; Shepard, K. L.; Kim, P. Spin and valley quantum Hall ferromagnetism in graphene. *Nat. Phys.* **2012**, *8*, 550−556.

(43) Yu, G. L.; Jalil, R.; Belle, B.; Mayorov, A. S.; Blake, P.; Schedin, F.; Morozov, S. V.; Ponomarenko, L. A.; Chiappini, F.; Wiedmann, S.; Zeitler, U.; Katsnelson, M. I.; Geim, A. K.; Novoselov, K. S.; Elias, D. C. Interaction phenomena in graphene seen through quantum capacitance. *Proc. Natl. Acad. Sci. U. S. A.* **2013**, *110*, 3282−3286.

(44) Polshyn, H.; Zhou, H.; Spanton, E. M.; Taniguchi, T.; Watanabe, K.; Young, A. F. Quantitative Transport Measurements of Fractional Quantum Hall Energy Gaps in Edgeless Graphene Devices. *Phys. Rev. Lett.* **2018**, *121*, 226801.

(45) Smoleński, T.; Cotlet, O.; Popert, A.; Back, P.; Shimazaki, Y.; Knüppel, P.; Dietler, N.; Taniguchi, T.; Watanabe, K.; Kroner, M.; Imamoglu, A. Interaction-Induced Shubnikov-de Haas Oscillations in

Optical Conductivity of Monolayer MoSe$_2$. *Phys. Rev. Lett.* **2019**, *123*, 097403.

(46) Zhu, J.; Li, T.; Young, A. F.; Shan, J.; Mak, K. F. Quantum Oscillations in Two-Dimensional Insulators Induced by Graphite Gates. *Phys. Rev. Lett.* **2021**, *127*, 247702.

(47) Spanton, E. M.; Zibrov, A. A.; Zhou, H.; Taniguchi, T.; Watanabe, K.; Zaletel, M. P.; Young, A. F. Observation of fractional Chern insulators in a van der Waals heterostructure. *Science* **2018**, *360*, 62−66.

(48) Xie, Y.; Pierce, A. T.; Park, J. M.; Parker, D. E.; Khalaf, E.; Ledwith, P.; Cao, Y.; Lee, S. H.; Chen, S.; Forrester, P. R.; Watanabe, K.; Taniguchi, T.; Vishwanath, A.; Jarillo-Herrero, P.; Yacoby, A. Fractional Chern insulators in magic-angle twisted bilayer graphene. *Nature* **2021**, *600*, 439−443.

(49) Shimazaki, Y.; Schwartz, I.; Watanabe, K.; Taniguchi, T.; Kroner, M.; Imamoğlu, A. Strongly correlated electrons and hybrid excitons in a moiré heterostructure. *Nature* **2020**, *580*, 472−477.

(50) Zhang, L.; Wu, F.; Hou, S.; Zhang, Z.; Chou, Y.-H.; Watanabe, K.; Taniguchi, T.; Forrest, S. R.; Deng, H. Van der Waals heterostructure polaritons with moiré-induced nonlinearity. *Nature* **2021**, *591*, 61−65.